encit 2020

ABCM Associação Brasileira de Engenharia e Ciências Mecânicas

18th Brazilian Congress of Thermal Sciences and Engineering
November 16–20, 2020 (Online)

ENC-2020-0058
INVERSE DESIGN OF HEAT SOURCE PATTERNS FOR TUMOR TREATMENTS VIA HYPERTHERMIA

1. João Magnus Bailuni de Bragança
2. Julia Latini Burgani
3. César Cunha Pacheco
Department of Mechanical Engineering, PGMEC/TEM, UFF, R. Passo da Pátria, 156, Niterói, Rio de Janeiro, Brazil
jbraganca@id.uff.br; juliaburgani@id.uff.br; cesarp@id.uff.br

Abstract. *The objective of this paper was to study the optimal design of heat sources for hyperthermia treatment of tumors in a realistic 3D brain geometry. This problem was recast by means of an inverse design problem, where the Pennes Bioheat Transfer Equation was used as the forward problem. This approach was successful in terms of parameter optimization. The inverse problem was solved by defining an ideal temperature distribution, in which a small temperature increase was present within the tumor region. The mathematical model, as well as the desired temperature profile, were manipulated in terms of the temperature increase, instead of the absolute temperature, simplifying the analysis. The brain model contains an intraventricular tumor and was obtained from magnetic resonance images (MRI). The Pennes equation was solved using OpenFOAM, while the inverse problem was solved using the Levenberg-Marquardt method. This methodology is also very versatile, allowing for different heating models to be selected, including ultrasound heating, which is considered as one of the methods of choice for hyperthermia. It also allows for medical professionals to design patient-specific thermal doses, improving the success rate of the treatment.*

Keywords: *bioheat transfer, inverse design, numerical solution, tumor treatment*

1. INTRODUCTION

Cancer is a major public health problem worldwide (Siegel *et al.*, 2018). According to Bray *et al.* (2018), there were 18.1 million new cases reported in 2018, with 9.6 million estimated deaths. The number of cases is expected to be close to 25 million over the next two decades, with greatest impact over low- and middle-income countries. Several tissues in the human body are likely to develop this disease (cf. Fig. 1).

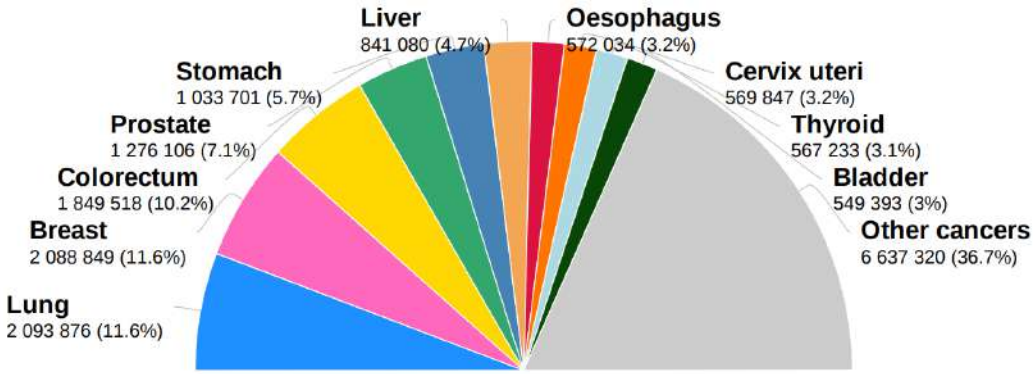

Figure 1. Estimated world cancer incidence proportions by major sites, in both sexes combined, 2018. Source: Global Cancer Observatory (GCO-WHO). Available at: https://gco.iarc.fr/today/online-analysis-pie

The medical community has been working both on the developing different treatments and on improving the already known. In general, these treatments can be divided in invasive and non-invasive. Within the non-invasive group, which includes procedures like chemotherapy and radiotherapy, thermotherapy has been shown to be a good alternative (Pacheco, 2018). Thermotherapy consists in the application of heat or cold for the purpose of changing temperature of soft tissues seeking therapeutical effects. The majority of thermotherapies are designed to deliver the thermal doses to a target tissue volume with minimal impact on surrounding tissues, being classified according to its heating intensity (Hildebrandt *et al.*, 2002): in thermal ablation, tumoral tissue is heated from 50 up to 80°C for 1 to 2 minutes, causing tissue necrosis; in hyperthermia a 42 to 45°C heating takes place over a longer period of time (which can be up to 60 min). This second

treatment can act as a sensitizer for other types of treatment, enhancing blood perfusion, permeability in vessels and therefore, a better and homogeneous drug delivery (Seynhaeve *et al.*, 2020). It can also induce apoptosis, a form of programmed cell death in a more orderly process compared with necrosis.

Ultrasound heating technology seems to be a good alternative for generating heat through mechanical friction (mechanical waves). In a non-intrusive manner, it has the advantage of heating not only superficial regions, but also the internal ones with beam focal and shape adjustment (Zhu *et al.*, 2019), with penetration depth ranging from less than 1 cm up to about 20 cm (Sethi and Chakarvarti, 2015). However, it can not penetrate through tissues that contain air (e.g., respiratory tract and gastrointestinal tract) and is subjected to high bone absorption. Concomitantly, internal tissue temperature can be indirectly measured *in situ* using PRF-Shift Magnetic Resonance Thermometry (Pacheco *et al.*, 2016). It is one of the most widely used technique due to its robustness and near tissue-independency (Ishihara *et al.*, 1995), where the temperature increase values are measured using gradient-echo (GRE) image sequences.

Several inverse bioheat transfer methods were applied to estimate the thermophysical and geometrical properties of tumors in 2D and/or 3D models. Malinen *et al.* (2003) designed an optimal thermal dose for ultrasound surgery in a 2D domain. The model contemplated the phases and amplitudes of the transducers instead of pre-focused ultrasound fields. The method used is based on a feedforward temperature controller, and it succeeded in keeping the thermal dose in healthy tissues low. Paruch and Majchrzak (2007) used the evolutionary method coupled with the multiple reciprocity boundary element method to estimate not only thermal parameters of tumors but also its size and location in a 3D domain. The algorithm diverged for some specific cases or another solution was obtained. Agnelli *et al.* (2010) have used inverse problems to estimate the metabolic heat source intensity and geometrical parameters of a tumor in 2D and 3D domains. The Pattern Search method was implemented, where the temperature profiles were obtained by infrared thermography. The results showed good agreement with actual and predicted parameter even when 5% and 10% random noises were added to the input data. Even so, experiments for deep tumors were not performed. None of the authors cited above have used a realistic 3D brain model.

2. FORWARD PROBLEM

2.1 Physical Model

2.1.1 3D Brain Model Reconstruction

A realistic 3D model was created based on MRI images obtained from Antônio Pedro University Hospital, of the Federal Fluminense University in Niterói. The process is performed in two main steps. First, the skull, skin and some underlying tissues are removed using Mango software, so that only the region of interest (brain with tumor) remains. Figure 2 illustrates this procedure. This output was then processed with 3D Slicer software in order to separate the regions of interest by means of the contrast of the MRI images. There were three main regions of interest: healthy tissue, tumoral tissue and cerebrospinal fluid. A frame of the region separation with 3D Slicer can be seen in Fig. 3. The two solid regions were then exported as STL files in order to generate the geometry, as it can be seen in Fig. 4.

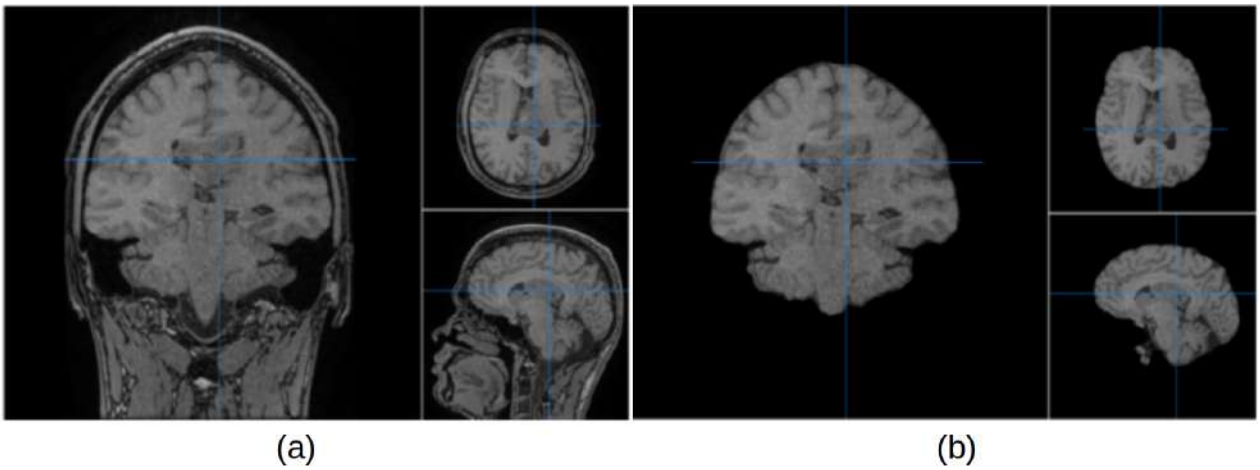

Figure 2. Undesired regions removal procedure with Mango software; a) before; b) after.

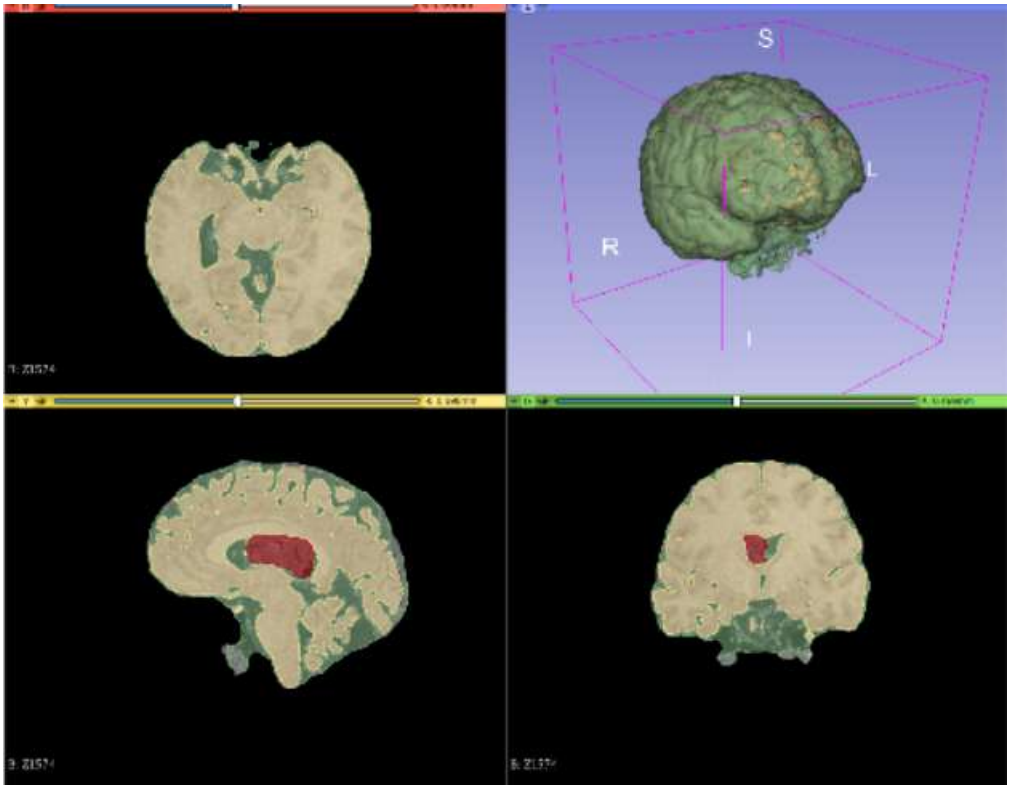

Figure 3. Brain 3D reconstruction in three main regions: healthy tissue (yellow), tumoral tissue (red) and cerebrospinal fluid (green) using 3D Slicer software.

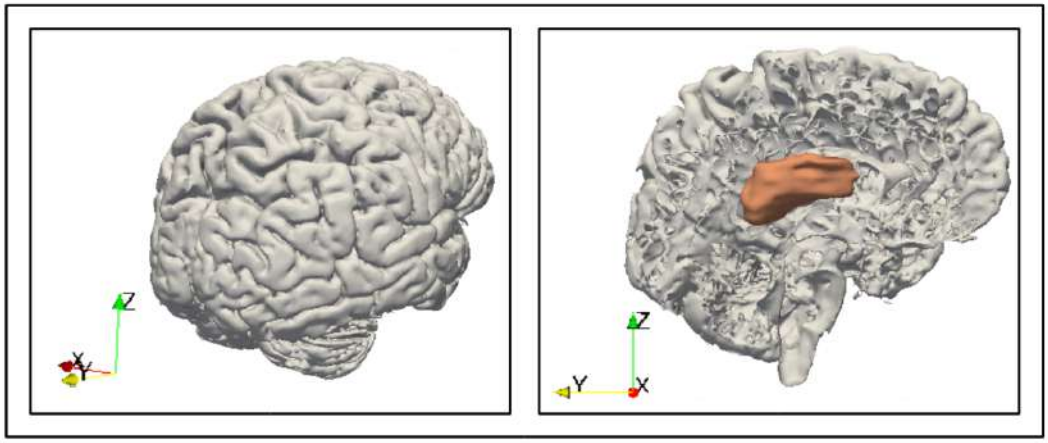

Figure 4. Healthy (gray) and tumoral (orange) tissue STL.

2.2 Mathematical Model

The energy balance over the spatial domain Ω is mathematically described using the steady bioheat transfer model by Pennes (1948) (cf. Eq. (1)), which is up to date one of the most widely used bioheat transfer models, due to its simplicity. The model depends on thermophysical parameters such as the tissue density ρ; the specific heat at constant pressure c_p; and the thermal conductivity κ. It also relies on physiological parameters, such as the blood perfusion rate ω_b; the blood density and specific heat at constant pressure ρ_b and c_b, respectively; the arterial temperature T_a; and the metabolic heat generation g_m. Finally, the model also considers an external volumetric heat generation term g_h, due to the hyperthermia process. This external heating acts in order to produce a temperature increase from the baseline temperature $T_0(\mathbf{x})$, i.e. the tissue temperature prior to the onset of hyperthermia heating. In order to obtain an unique solution for this governing equation, one must pose a boundary condition. In this work, it is assumed that the hyperthermia treatment takes place far from the boundaries, so that temperatures in the region are not expected to deviate from the baseline values (cf. Eq. (2)).

$$\nabla \cdot [\kappa \nabla T(\mathbf{x})] + \omega_b \rho_b c_b [T_a - T(\mathbf{x})] + g_h(\mathbf{x}) + g_m(\mathbf{x}) = 0, \qquad \mathbf{x} \in \Omega; \tag{1}$$

$$T(\mathbf{x}) = T_0(\mathbf{x}), \qquad \mathbf{x} \in \partial\Omega. \tag{2}$$

Considering that MRI temperature mapping techniques reveal temperature variations $\Delta T(\mathbf{x}) = T(\mathbf{x}) - T_0(\mathbf{x})$ instead of absolute temperature $T(\mathbf{x})$ (Pacheco, 2018), the problem must be recast in terms of $\Delta T(\mathbf{x})$ in the following manner:

$$T(\mathbf{x}) = T_0(\mathbf{x}) + \Delta T(\mathbf{x}). \tag{3}$$

By assuming that no temperature increase will take place in the absence of external heating (i.e. $g_h = 0 \Rightarrow \Delta T = 0$), it is possible to apply Eq. (3) to Eqs. (1)-(2) and separate them into two distinct models, one for $T_0(\mathbf{x})$ and one for $\Delta T(\mathbf{x})$. For the purposes of this paper, the model for $T_0(\mathbf{x})$ is not addressed herein. The latter is given by:

$$\nabla \cdot [\kappa \nabla(\Delta T(\mathbf{x}))] - \omega_b \rho_b c_b \Delta T(\mathbf{x}) + g_h(\mathbf{x}) = 0; \tag{4}$$

$$\Delta T(\mathbf{x}) = 0, \qquad \mathbf{x} \in \partial\Omega. \tag{5}$$

This formulation does not depend on the baseline temperature $T_0(\mathbf{x})$, the metabolic heat generation and arterial temperature, being thus less dependent on physiological parameters, which vary from patient to patient. The absolute temperature can be post-processed from this formulation with irrelevant computational cost (Pacheco *et al.*, 2016; Pacheco, 2018).

2.3 Heating Model

In this work, a generic heating model was assumed, being described in terms of a Gaussian expression defined by up to seven parameters: focal position ($\bar{x}$, $\bar{y}$, $\bar{z}$), aperture in each direction (σ_x, σ_y, σ_z) and intensity (g_0). Thus, the heat source term is given by:

$$g_h(x, y, z) = g_0 \exp\left\{ -\frac{1}{2}\left[\frac{(x-\bar{x})^2}{\sigma_x^2} + \frac{(y-\bar{y})^2}{\sigma_y^2} + \frac{(z-\bar{z})^2}{\sigma_z^2} \right] \right\}. \tag{6}$$

This model was chosen in order to mimick typical heating patterns in thermal therapies. One can notice that the heating is more intense within the tumor at the focal point $(x, y, z) = (\bar{x}, \bar{y}, \bar{z})$, while it gets weaker as it gets further from that point. For a better understanding, Fig. 5 compares three different cases in a 1D domain where the effects of parameter variations are noticed.

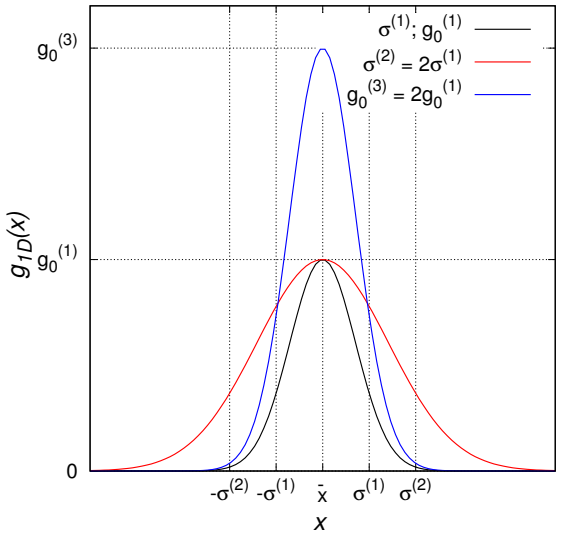

Figure 5. 1D heating model for three different cases.

2.4 Numerical Solution

The mathematical model (Eqs. (4)-(5)) presented above was solved numerically in OpenFOAM (Open Source Field Operation and Manipulation) v.5.0. OpenFOAM is a C++ toolbox for computational fluid dynamics, heat transfer, among others. It can be used to apply the finite volume method to solve partial differential equations (Weller *et al.*, 1998). The solver used was the laplacianFoam, which is a library for solving diffusion problems with a source term. The user may set a constant scalar diffusion rate (DT), which is equivalent to the thermal diffusivity. The first order implicit Euler method was considered in a pseudo-transient simulation, with the Gaussian integration to discretize all spatial derivatives.

The geometry generated in the previous section was used as input for snappyHexMesh, a meshing tool available in OpenFOAM v5.0. Three refinement levels were proposed for a convergence test, duplicating the number of control volumes at each test. The parameters were chosen arbitrarly to solve the forward problem, and the differences between the second and third grids results were less than 1,41%. The mesh contains 188,560 volumes and a detailed refinement treatment at the region of interest (tumor) was performed. Figure 6 shows a sagittal view of the grid. Although its majority seems to be structured, the grid generated with snappyHexMesh contains a few prisms, tetrahedral and polyhedral cells due to the surfaces with complex shapes.

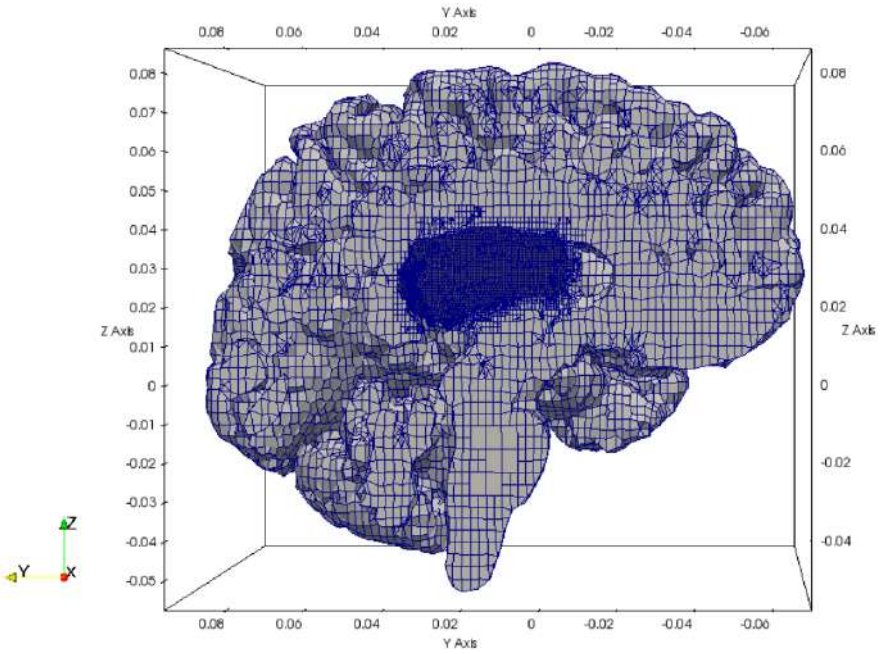

Figure 6. Sagittal view of brain's mesh, with 188,560 volumes.

3. INVERSE PROBLEM

If in the forward problem the goal is to find the effects obtained from known causes, in the inverse problem, the causes (or parameters) are to be determined from experiments or an ideal solution. The sought parameters are arranged in the vector $\mathbf{a}$ (cf. Eq. 7), which is to be identified for a desired temperature increase distribution.

$$\mathbf{a} = [g_0 \quad \bar{x} \quad \bar{y} \quad \bar{z} \quad \sigma_x \quad \sigma_y \quad \sigma_z]^T. \tag{7}$$

In order to perform this parameter estimation, it is assumed that the temperature values along the mesh can be obtained in the form of the vector function $\mathbf{f}(\mathbf{a})$, by appropriately solving the forward problem. Also, the desired temperature increase field is stored in the vector $\mathbf{y}$ and assumed to be zero everywhere except for the tumor region, where a increase of 5 °C was imposed. Therefore, the goal of the inverse analysis is to find $\mathbf{a}$ which provides the best approximation of the desired temperature increase. In this work, this task is performed by minimizing the ordinary least squares norm:

$$S(\mathbf{a}) = \| \mathbf{y} - \mathbf{f}(\mathbf{a}) \|^2, \tag{8}$$

This nonlinear least squares problem is solved by using the Levenberg-Marquardt method (cf. Eqs. (9)-(10)) (Ozisik and Orlande (2000); Levenberg (1944); Marquardt (1963)), which was programmed using FORTRAN90 language and coupled to the OpenFOAM solver using Linux shell script.

$$\mathbf{a_{i+1}} = \mathbf{a_i} + (\mathbf{J_i}^T\mathbf{J_i} + \lambda\mathbf{\Theta})^{-1}\mathbf{J_i}^T(\mathbf{y} - \mathbf{f_i}); \tag{9}$$

$$\mathbf{\Theta} = \text{diag}(\mathbf{J}^T\mathbf{J}). \tag{10}$$

In the Levenberg-Marquardt method, $\mathbf{J}$ is the sensitivity matrix and $\lambda\mathbf{\Theta}$ is a damping factor that seeks to alleviate possible instabilities, due to the ill-posed nature of the inverse design problem. $\mathbf{J}$ basically describes how sensible the solution is related to the parameters, helping the method to find a better guess. It is calculated by means of a forward finite difference approximation around the current estimate. Initially, $\lambda = 10^{-3}$. If the solution converges, it gets divided by 10 and completes an iteration, else, it is multiplied by 10 and returns to the parameter estimation. The inverse solution can only proceed to the next iteration after $S(\mathbf{a_{i+1}}) < S(\mathbf{a_i})$. If it can not find any better solutions than the previous, the code is

paused manually. It is important to have in mind that this method will not work if the variation of two or more parameters produces the same effect in the solution. In other words, **J** must be full rank in order to estimate all the parameters. If any of the columns of **J** can be written as a linear combination of the others, the method does not work. More specifically, in order to be able to achieve the sought solution, the desired parameters must be linearly independent (Ozisik and Orlande, 2000), which was shown to be the case for the present investigation. Because the Levenberg-Marquardt method may be highly dependent on the initial guess, a test for three different cases (T[1], T[2] and T[3]) was performed, varying arbitrarly all the parameters. Figure 7 ilustrates the location of the focal point ($\bar{x}\ \bar{y}\ \bar{z}$) in each test and all the initial conditions can be seen in Tab. 1. The tests basically converged to the same results, being the greater variation of 1.46% in the estimative of σ_x between tests T[1] and T[2]. The norm $S(\mathbf{a})$ variated less than 0.08% between all tests.

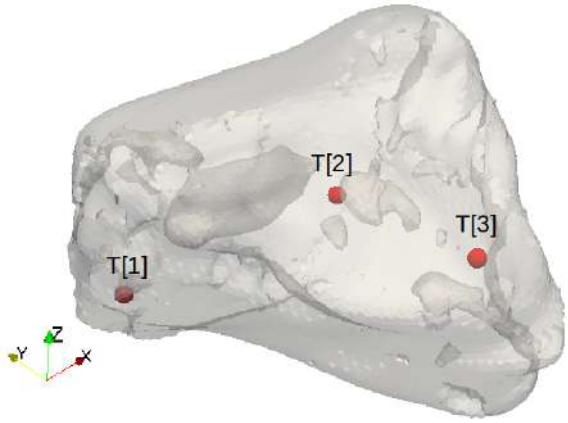

Figure 7. Focal point of the heat source for the tests T[1], T[2] and T[3].

Table 1. Initial condition of the parameters estimated in tests T[1], T[2] and T[3].

	g_0 [W/m^3]	$\bar{x}$ [m]	$\bar{y}$ [m]	$\bar{z}$ [m]	σ_x [m]	σ_y [m]	σ_z [m]
T[1]	6.443×10^{-2}	0.984	1.030	1.020	3.394×10^{-4}	2.115×10^{-3}	4.448×10^{-4}
T[2]	1.033×10^{-1}	1.000	1.020	1.029	9.381×10^{-3}	1.300×10^{-2}	5.245×10^{-3}
T[3]	5.916×10^{-1}	1.001	1.003	1.034	5.220×10^{-2}	1.181×10^{-1}	3.991×10^{-2}

4. RESULTS AND DISCUSSION

In order to solve numerically all mathematical models posed above, physical properties of biological tissues must be considered. The values for the healthy tissue are obtained from Hasgall *et al.* (2018) database and shown in Tab. 2. This table also contains the assumed value for the blood perfusivity rate for the healthy tissue, also obtained from Hasgall *et al.* (2018). As for the tumorous tissue, the thermophysical properties were assumed to be the same, while the blood perfusivity was assumed to be four times larger, according to Liu and Xu (2000). All cases runned with Intel Core TM i7-6700 CPU @ 3.40GHz $\times$ 8 processor and 32GB RAM desktop.

Table 2. Numerical values for the parameters of the bioheat transfer model (Hasgall *et al.*, 2018).

Properties	ρ [kg/m^3]	c_p [J/kg°C]	κ [W/m°C]	ω_b [1/s]
Value	1046	3630	0.51	9.7×10^{-3}

4.1 Case A: 1D Preliminar Test

To test the proposed methodology, a preliminary 1D case was first proposed. In this case, Eq. (6) is reducted to Eq. (11). The domain size is assumed to be $L = 0.1$ m, with origin at $x = 1$ m and center at $x = 1.05$ m. Here, the ideal solution is represented by a uniform increase of 5°C within the whole tumor (centered in the domain, and 0.02 m long), with no variation in the rest of the domain temperature.

$$g_h(x) = g_0 \exp\left[-\frac{(x - \bar{x})^2}{2\sigma_x^2} \right]. \tag{11}$$

4.1.1 Case A1: Without Perfusion Term

First, a scenario assuming no blood perfusion was considered. The obtained result is shown at Fig. 8, with the associated parameters being given by Tab. 3. The running time for this case was of 15min40s. As it can be seen, the algorithm succeded in approximate as much as possible the desired temperature increase profile. It is important to point out that due to the nature of the selected heat source, the inverse analysis cannot be expected to return a set of parameters that perfectly produces the desired distribution.

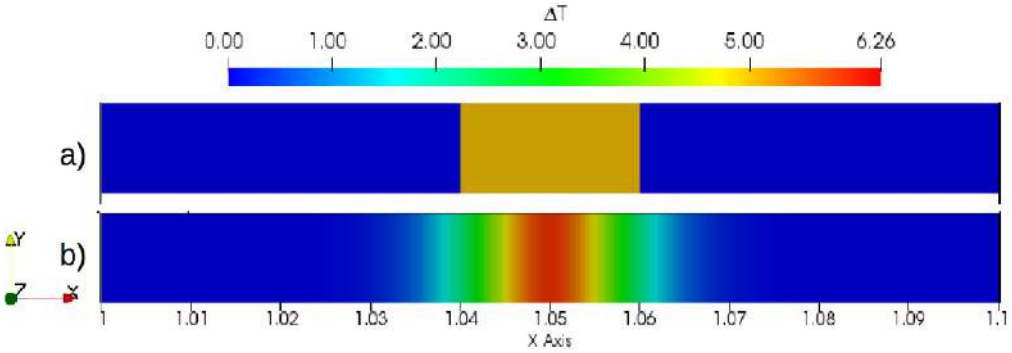

Figure 8. Comparison between 1D ideal solution and 1D steady solution found by the algorithm; a) ideal solution; b) numerical solution without perfusion term.

Table 3. **Case A1** results.

S	$\bar{x}$ [m]	σ_x [m]	g_0 [W/m^3]
11.958	1.050	5.911×10^{-3}	8.026×10^{-2}

4.1.2 Case A2: With Perfusion Term

After obtaining results for **Case A1**, we proceed to perform a new 1D scenario, this time including the effect of the blood perfusion in the tissue. The results are shown in Fig. 9, with the associated parameters given by Tab. 4. The required computational time for this case was of 6min58s. The ΔT distribution and the residual $r_i = f_i(\mathbf{a}) - y_i$ of both cases are shown in Fig. 10, where it can be noticed how the presence of the perfusion term ω_b may predict paremeters that are more harmful to the brain. Despite the bigger aperture σ_x for **Case A1**, the healthy tissue mantains its temperature below the one prescribed for hyperthermia, and it also represents a more homogeneous heating. An evaluation of the maximum temperature of both cases showed a 5.54% higher estimation of ΔT for **Case A2** when compared with **Case A1**. Figure 11 also ilustrates how the presence of the perfusion term produces a less conservative scenario for the prediction of the heat source g_h.

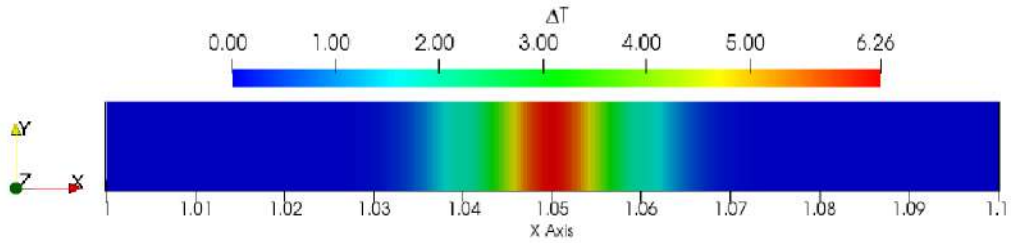

Figure 9. 1D numerical solution with perfusion term.

Table 4. **Case A2** results.

S	$\bar{x}$ [m]	σ_x [m]	g_0 [W/m^3]
14.549	1.050	5.293×10^{-3}	5.214×10^{-1}

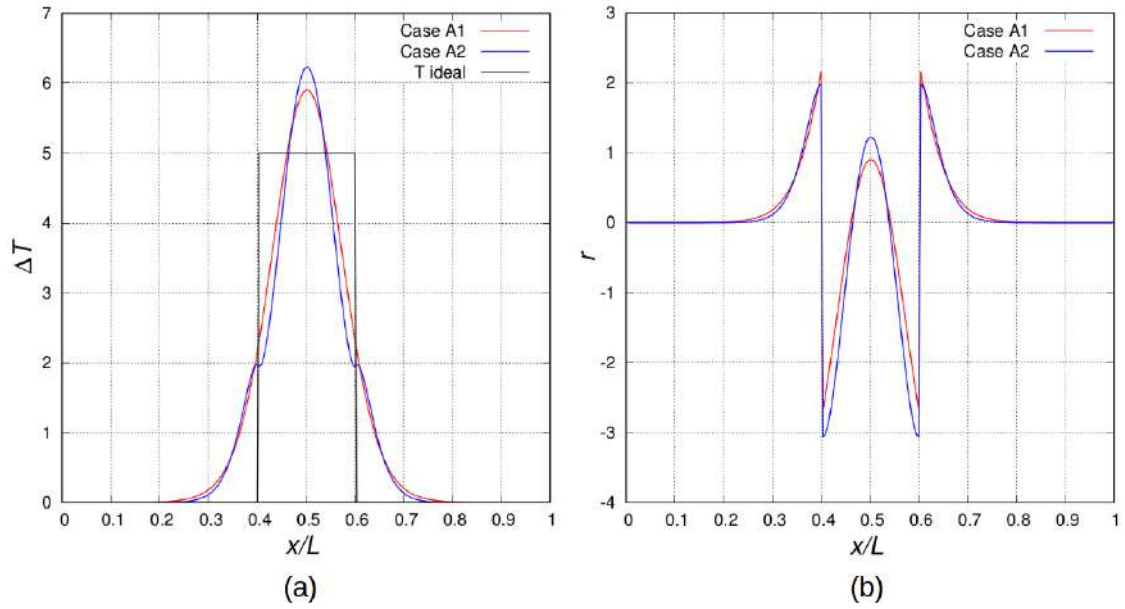

Figure 10. Comparison between cases A1 and A2 for: a) ΔT distribution; b) residual r.

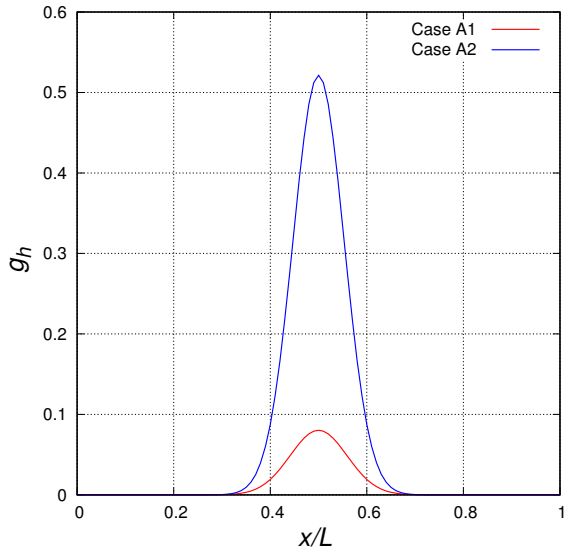

Figure 11. g_h distribution for cases A1 and A2.

4.2 Case B: 3D Solution

Because of the better results achieved for **Case A1** in terms of preservation of the healthy tissue, the 3D case will not consider the effects of blood perfusion. Analogous to **Case A**, the ideal solution considers a fictional situation where the whole tumor temperature is exactly $5°$C above the healthy tissue temperature. The results can be seen in Fig. 12 and Tab. 5. This solution reached convergence in 2h58min.

Table 5. **Case B** results.

g_0 [W/m^3]	$\bar{x}$ [m]	$\bar{y}$ [m]	$\bar{z}$ [m]	σ_x [m]	σ_y [m]	σ_z [m]
9.749×10^{-2}	1.001	1.020	1.029	9.826×10^{-3}	1.339×10^{-2}	5.254×10^{-3}

Because thermal diffusion is uniform in the human tissue, it is merely impossible to get the exact results expected in the ideal solution. That is the reason why S is always greater than zero. Differences between **Case A** and **Case B** results in terms of accuracy and computational cost are explained by the higher complexity of **Case B**. Both brain and tumor geometries and mesh are more complex; and there are four parameters more to estimate.

Case B ran with perfusion term turned off because it was supposed to represent a more conservative scenario. It can be

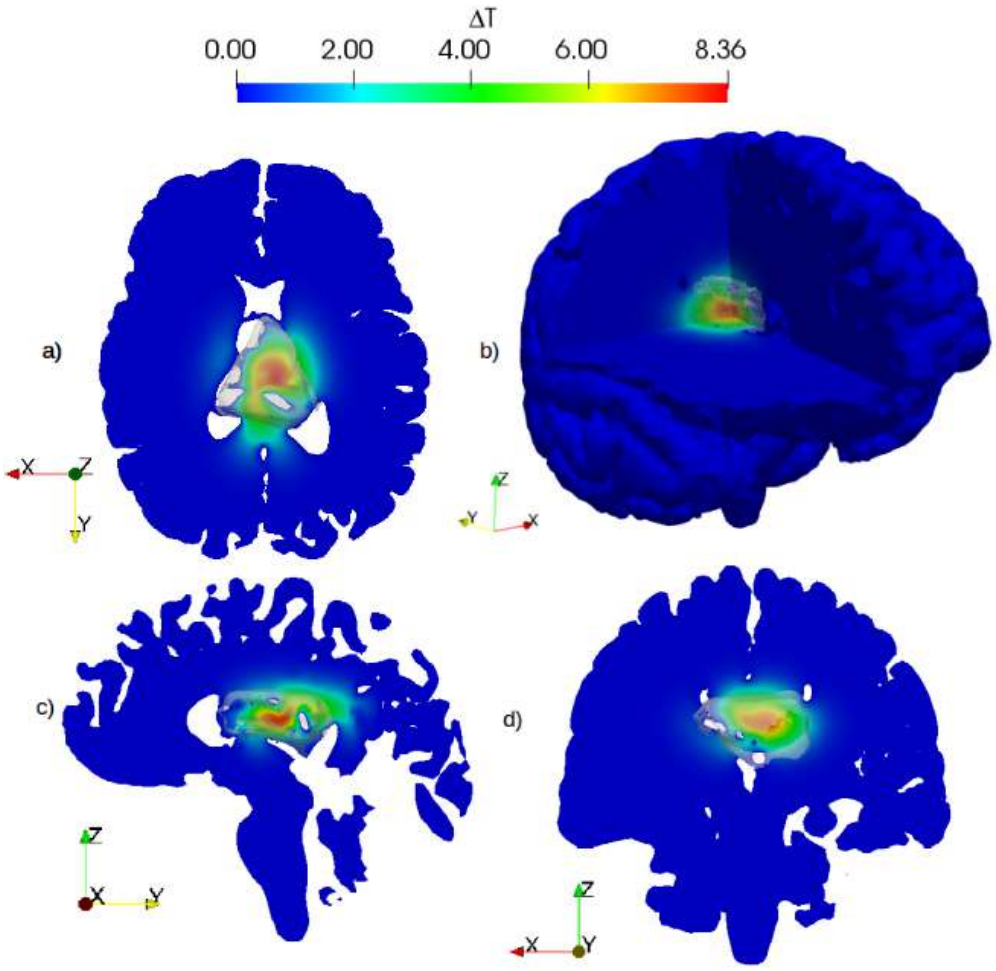

Figure 12. 3D numerical solution; a) axial view; b) 3D view; c) sagittal view; and d) coronal view.

clearly seen when comparing both g_0 solutions for **Case A1** and **Case A2**, where the presence of perfusion should delay the heating. Neglecting the internal circulation of cerebrospinal fluid and its heat conduction/convection can also be seen as a conservative hypothesis. Including the fluid domain would bring unnecessary complexity at this stage.

These results do not contemplate physiological responses neither probable differences between patients particular characteristics (like tissue physical properties or tumor form and location), although statistical analysis can be made. Additional boundary conditions may be applied to avoid unnecessary heating of healthy tissue.

5. CONCLUSIONS

The approach considered in this work succeeded in terms of parameters optimization. It also has the advantage of being appliable to every tissue from the body, once the MRI images are given. Free available softwares for MRI manipulation (Mango and 3D Slicer) are carrying out the role of creating realistic 3D models of biological tissues. Hence, the method presented in this paper can be helpful in finding patient-specific thermal doses. The presence of cerebrospinal fluid, the physiological responses and more detailed properties variations may interfere in the solution. Therefore, studying these influences on the final solution would increase the model robustness. If the considered tumor was more superficial, caution should be taken to the boundary conditions. A future step to this work shall consider including a more detailed heating model, an expanded version of the one presented in this work that accounts for all variables of a realistic heating procedure (i.e. ultrasound, radio frequency, etc).

6. ACKNOWLEDGEMENTS

The authors would like to thanks Antônio Pedro University Hospital, from Federal Fluminense University and the Brazilian Agency CAPES.

7. REFERENCES

Abushkin, I., Denis, A., Vasiliev, I., Lappa, A., Privalov, V., Gavrilova, O., Lapin, V., Romanova, O. and Galiulin, M., 2018. "Laser thermotherapy of vascular tumors in children under ultrasound control." In *2018 International Conference Laser Optics (ICLO)*. pp. 468–468.

Agnelli, J., Barrea, A. and Turner, C., 2010. "Tumor location and parameter estimation by thermography". *Mathematical and Computer Modelling*, Vol. 53, pp. 1527–1534.

Bray, F., Ferlay, J., Soerjomataram, I., Siegel, R.L., Torre, L.A. and Jemal, A., 2018. "Global cancer statistics 2018: Globocan estimates of incidence and mortality worldwide for 36 cancers in 185 countries". *American Cancer Society Journals*, Vol. 68, pp. 394–424.

Hasgall, P.A., Gennaro, F.D., Baumgartner, C., Neufeld, E., Lloyd, B., Gosselin, M.C., Payne, D.K.A. and Kuster, N., 2018. "It'is database for thermal and electromagnetic parameters of biological tissues". <itis.swiss/database>.

Hildebrandt, B., Wust, P., Ahlers, O., Dieing, A., Sreenivasa, G., Kerner, T., Felix, R. and Riess, H., 2002. "The cellular and molecular basis of hyperthermia". *Critical Reviews in Oncology/Hematology*, Vol. 43, pp. 33–56.

Ishihara, Y., Calderon, A., Watanabe, H., Okamoto, K., Suzuki, Y., Kuroda, K. and Suzuki, Y., 1995. "A precise and fast temperature mapping using water proton chemical shift". *Magnetic Resonance in Medicine*, Vol. 34, pp. 814–823.

Levenberg, K., 1944. "A method for the solution of certain non-linear problems in least squares". *The Quarterly of Applied Mathematics*, Vol. 2, pp. 164–168.

Liu, J. and Xu, L.X., 2000. "Boundary information based diagnostics on the thermal states of biological bodies". *International Journal of Heat and Mass Transfer*, Vol. 43, pp. 2827–2839.

Malinen, M., Huttunen, T. and Kaipio, J., 2003. "Thermal dose optimization method for ultrasound surgery". *Physics in Medicine and Biology*, Vol. 48, pp. 745–762.

Marquardt, D., 1963. "An algorithm for least-squares estimation of nonlinear parameters". *Journal of the Society for Industrial and Applied Mathematics*, Vol. 11, pp. 431–441.

Ozisik, M.N. and Orlande, H.R.B., 2000. *Inverse Heat Transfer: Fundamentals and Applications*. Taylor & Francis, Florida, USA, 1st edition.

Pacheco, C.C., 2018. *Estimativa de variáveis de estado na termometria por ressonância magnética aplicada ao tratamento de tumores*. Ph.D. thesis, COPPE/UFRJ, Rio de Janeiro, Brasil.

Pacheco, C.C., Orlande, H.R.B., Colaco, M.J. and Dulikravich, G.S., 2016. "State estimation problems in prf-shift magnetic resonance thermometry". *International Journal of Numerical Methods for Heat & Fluid Flow*, Vol. 28, pp. 6–8.

Paruch, M. and Majchrzak, E., 2007. "Identification of tumor region parameters using evolutionary algorithm and multiple reciprocity boundary element method". *Engineering Applications of Artificial Intelligence*, Vol. 20, pp. 647–655.

Pennes, H.H., 1948. "Analysis of tissue and arterial blood temperatures in the resting human forearm". *Journal of Applied Physiology*, Vol. 1, pp. 93–122.

Sethi, M. and Chakarvarti, S.K., 2015. "Hyperthermia techniques for cancer treatment: A review". *International Journal of PharmTech Research*, Vol. 8, pp. 974–4304.

Seynhaeve, A., Amin, M., Haemmerich, D., van Rhoon, G. and ten Hagen, T., 2020. "Hyperthermia and smart drug delivery systems for solid tumor therapy." *Advanced Drug Delivery Reviews*. In Press.

Siegel, R.L., Miller, K.D. and Jemal, A., 2018. "Cancer statistics, 2018". *CA: A Cancer Journal for Clinicians*, Vol. 68, pp. 7–30.

Weller, H.G., Tabor, G., Jasak, H. and Fureby, C., 1998. "A tensorial approach to computational continuum mechanics using object-oriented techniques". *Computers in Physics*, Vol. 12, pp. 894–1866.

Zhu, L., Altman, M.B., Laszlo, A., Straube, W., Zoberi, I., Hallahan, D.E. and Chen, H., 2019. "Ultrasound hyperthermia technology for radiosensitization". *World Federation for Ultrasound in Medicine & Biology*, Vol. 45, pp. 1025–1043.

8. RESPONSIBILITY NOTICE

The authors are solely responsible for the printed material included in this paper.